Available online at www.sciencedirect.com
SCIENCE DIRECT®
Journal of Computational Physics 192 (2003) 523–545
JOURNAL OF COMPUTATIONAL PHYSICS
www.elsevier.com/locate/jcp

Estimation of resonant frequencies and quality factors from time domain computations

Thomas Rylander [a,*], Tomas McKelvey [b], Mats Viberg [b]

[a] Center for Computational Electromagnetics, Department of Electrical and Computer Engineering, University of Illinois at Urbana-Champaign, Urbana, IL 61801-2991, USA
[b] Department of Signals and Systems, Chalmers University of Technology, 412 96 Göteborg, Sweden

Received 28 March 2003; received in revised form 24 July 2003; accepted 24 July 2003

Abstract

A new frequency domain subspace algorithm for the estimation of resonant frequencies and quality factors given the output from time domain computations is developed and tested. It applies the discrete Fourier transform to the time domain signal and the estimates are computed from the frequency data within the frequency band of interest. Thus, out-of-band disturbances are suppressed through a band-pass filtering operation in frequency domain, which is free from the transient effects that are inevitable for standard time domain filtering techniques. We also propose an efficient procedure to generate short time domain excitations with an a priori specified frequency spectrum. By combining such excitations with the frequency domain subspace algorithm, we estimated to high accuracy the lowest 167 resonant frequencies of a three-dimensional bow-tie microwave resonator given two separate time domain computations with, in total, 23,000 time steps. A free-space computation for a cavity with an aperture shows that the estimation algorithm can be used to efficiently and accurately extrapolate time domain signals. The tests show that it is possible to reduce the overall computation time by several orders of magnitude for systems with undamped or weakly damped modes. It operates as a post-processing step and, thus, decouples the estimation of frequencies and amplitudes from the time domain solver which offers a considerable flexibility.

PACS: 43.60.Uv; 02.30.Nw; 40.20.−q

Keywords: Estimation of harmonics; Resonant frequency; Quality factor; System identification; Temporal excitation; Time domain finite element method; Finite-difference time-domain; Maxwell's equations

1. Introduction

Time domain computations for electromagnetic problems are currently developing at a high pace. The finite-difference time-domain (FDTD) scheme [1,2] has found great popularity since it is easy to understand

* Corresponding author. Tel.: +1-217-333-1202; fax: +1-217-333-5962.
E-mail addresses: tryl@uiuc.edu (T. Rylander), mckelvey@s2.chalmers.se (T. McKelvey), viberg@s2.chalmers.se (M. Viberg).

0021-9991/$ - see front matter © 2003 Elsevier B.V. All rights reserved.
doi:10.1016/j.jcp.2003.07.011

and program. Although the FDTD scheme was introduced almost four decades ago, it is only relatively recently that other numerical methods, e.g., the finite element method (FEM) and boundary element method (BEM), have been formulated and used successfully for time domain computations in electromagnetics. The books by Jin [3] and Chew et al. [4] give an account of time domain FEM and recent advances in time domain BEM, respectively. One reason for the increasingly high interest in time domain computations is that one single simulation can provide the response of an electromagnetic system in a wide frequency band, whereas a frequency domain formulation uses one computation for each separate frequency. However, the extraction of frequency domain data given the output from a time domain computation remains problematic. In particular, cases with undamped and weakly damped modes are challenging, especially for closely spaced eigenfrequencies. A time domain computation requires that the eigenfrequencies are extracted from the time domain data. In order to reduce the computational cost, it is highly desirable to use as few time steps as possible to recover the sought frequency data in an a priori selected frequency band.

In signal processing, the estimation of damped and undamped sinusoidal signals from measurements is an extensively studied problem. The books by Kay [5] and Stoica and Moses [6] give a good overview of existing techniques. However, the estimation of closely spaced frequencies is still a challenging problem, especially when the number of time samples is scarce and/or the number of spectral lines is large. Existing estimators can coarsely be characterized as non-parametric and parametric ones. Non-parametric methods search for peaks in a parameter-free spectral estimate. The resolution of such methods is limited by the available data length. The purpose of parametric methods is to reduce the amount of data required for a given resolution. The computations typically involve the following two steps: First, model parameters, e.g., auto-regressive polynomial coefficients, are estimated based on sample covariances computed from data. The second step involves computing the frequencies, and it can be implemented in various ways: (1) root-finding of polynomials, (2) eigenvalue calculations or (3) peak finding in a model associated pseudo-spectrum. Some of the parametric techniques are applicable if the number of frequencies is low or moderate, e.g., Prony's method has been exploited for electromagnetic computations by Ko and Mittra [7] and Pereda et al. [8], while Shaw and Naishadham [9] used an ARMA modeling for resonant electromagnetic structures. Also the method referred to as Padé approximation [10] in the electromagnetic literature [11,12] is based on ARMA modeling, but using frequency domain data. In the signal processing literature, Padé approximation usually refers to a special technique for time domain ARMA modeling, see e.g. [6]. For problems with a large number of frequencies which are also closely spaced, only high resolution techniques such as Kung's method [13], ESPRIT [14] or MUSIC [15] can yield satisfactory results. For electromagnetic systems, Bi et al. [16] applied the MUSIC method to the analysis of resonators, and Liu et al. [17] used the ESPRIT to compute multi-mode dispersive modal parameters for multi-conductor transmission lines. Though the mentioned subspace-based frequency estimation techniques offer high resolution, their use is limited to relatively small numbers of spectral lines and moderately sized data sets because of computational complexity and numerical difficulty for large problems. The application of parametric techniques to electromagnetic problems is non-trivial since Maxwell's equations support an unlimited number of eigenfrequencies, and at higher frequencies the spectrum gets increasingly dense. However, the part of the spectrum of main interest is discrete eigenfrequencies, and for these, it is appropriate to apply methods of high-resolution estimation.

In this paper we propose two different techniques for enabling high-resolution estimation of a limited number of frequency components. First, an accurate frequency domain subspace algorithm for fitting a state-space model (similar to [13]) to frequency domain data (as in [10–12]) is proposed and tested for problems in electromagnetics. The method is capable of giving exact results on noise-free data, regardless of the frequency separation. Further, it can simultaneously use multiple channels for the estimation in the case of imperfect data, where each channel can be a linear combination of all six field components sampled at

different spatial locations. The algorithm uses a subset of the discrete Fourier transform (DFT) data, where the selected DFT points reside in the frequency band of interest. Working on a subset of the DFT data corresponds to a band-pass filtering operation which suppresses out-of-band disturbances and it reduces the computational cost. Some preliminary tests with the proposed algorithm for undamped sinusoids are reported in [18]. Second, a technique for selecting the excitation signal is suggested, that limits the frequency support of the electromagnetic signals to the band of interest. This has the advantage of further reducing out-of-band interference, in addition to that offered by the Fourier transform pre-processing. In essence, the excitation selection is cast as a finite impulse response (FIR) filter design problem, for which a multitude of algorithmic tools exist. The two signal processing algorithms are general in nature and could be applied to any estimation situation involving harmonics which is found in, e.g., electrical circuit-theory, telecommunications, acoustics, solid mechanics and quantum mechanics.

2. Signal models

The field solution of an autonomous linear electromagnetic system can be represented as a superposition of eigenmodes with the complex eigenfrequencies $\beta_r = -\gamma_r + \mathrm{i}\omega_r$, where γ_r is the damping and ω_r is the angular frequency for the rth eigenmode. The characterization of such a system is normally formulated in terms of linear functionals $\mathscr{L}_p$ of, e.g., the electric field $\vec{E}(\vec{r}, t)$, where $p = 1, \ldots, P$. The output $\mathbf{y}(n) \in \mathbb{C}^{P\times 1}$ from a time domain computation can then be expressed as:

$$\mathbf{y}(n) = \begin{bmatrix} \mathscr{L}_1(\vec{E}(\vec{r}, n\Delta t)) \\ \mathscr{L}_2(\vec{E}(\vec{r}, n\Delta t)) \\ \vdots \\ \mathscr{L}_P(\vec{E}(\vec{r}, n\Delta t)) \end{bmatrix} \tag{1}$$

$$\triangleq \sum_{r=1}^{R} \mathbf{a}_r \mathrm{e}^{\beta_r n\Delta t} + \mathbf{w}(n), \tag{2}$$

where Δt denotes the time step and $n = 0, \ldots, N-1$ is the time index. The signal model (2) of the output (1) captures R resonances, and it is characterized by the complex frequencies $\beta_r \in \mathbb{C}$ and amplitudes $\mathbf{a}_r \in \mathbb{C}^{P\times 1}$ while $\mathbf{w}(n) \in \mathbb{C}^{P\times 1}$ corresponds to disturbances. In the case of simulated data such disturbances can originate from round-off errors, approximately solved systems of linear equations (by, e.g., iterative solvers) and other non-sinusoidal signals which are supported by the numerical scheme and unintentionally excited. The unknown frequencies β_r and amplitudes $\mathbf{a}_r$ are to be estimated. The model includes vector valued signals if $P > 1$ and real-valued signals is a special case.

To make the model unique we assume that the frequencies β_r are distinct, $\omega_r\Delta t \in (-\pi, \pi)$ and $\mathbf{a}_r \neq 0$ for all $r = 1, \ldots, R$. First, we treat the case when the disturbance term $\mathbf{w}(n)$ is zero and will later in Section 3.3 discuss the realistic case when $\mathbf{w}(n) \neq 0$. We introduce the matrix notation

$$\begin{aligned} &\mathbf{A} = \mathrm{diag}[\mathrm{e}^{\beta_1\Delta t}, \mathrm{e}^{\beta_2\Delta t}, \ldots, \mathrm{e}^{\beta_R\Delta t}] \in \mathbb{C}^{R\times R}, \\ &\mathbf{C} = [\,\mathbf{a}_1 \quad \mathbf{a}_2 \quad \cdots \quad \mathbf{a}_R\,] \in \mathbb{C}^{P\times R}, \quad \text{and} \\ &\mathbf{x}_0 = [\,1 \quad 1 \quad \cdots \quad 1\,]^{\mathrm{T}} \in \mathbb{R}^{R\times 1} \end{aligned} \tag{3}$$

as a preparation for the development of the estimation method. With this matrix notation we can compactly write $\mathbf{y}(n) = \mathbf{C}\mathbf{A}^n\mathbf{x}_0$. Note that the $\mathbf{A}$ matrix is diagonal and hence the R eigenvalues of $\mathbf{A}$ are $\mathrm{e}^{\beta_r\Delta t}$.

The representation of $\mathbf{y}(n)$ given by the matrix triple $(\mathbf{A}, \mathbf{C}, \mathbf{x}_0)$ defined in Eq. (3) is called a *realization* and it is *not* unique. Take an arbitrary non-singular matrix $\mathbf{T} \in \mathbb{C}^{R\times R}$. Then the matrix triple $(\tilde{\mathbf{A}}, \tilde{\mathbf{C}}, \tilde{\mathbf{x}}_0) \triangleq (\mathbf{T}^{-1}\mathbf{A}\mathbf{T}, \mathbf{C}\mathbf{T}, \mathbf{T}^{-1}\mathbf{x}_0)$ is also a valid realization of $\mathbf{y}(n)$, because $\mathbf{y}(n) = \tilde{\mathbf{C}}\tilde{\mathbf{A}}^n\tilde{\mathbf{x}}_0$. Note that the eigenvalues of $\tilde{\mathbf{A}}$ are still $e^{\beta_r \Delta t}$.

Given the matrix notation, a simple recursive formula for calculating $\mathbf{y}(n)$ exists, and it is called a *state-space model*

$$\begin{aligned} &\mathbf{x}(n+1) = \mathbf{A}\mathbf{x}(n), \quad \mathbf{x}(0) = \mathbf{x}_0, \\ &\mathbf{y}(n) = \mathbf{C}\mathbf{x}(n), \end{aligned} \tag{4}$$

where the state $\mathbf{x}(n) \in \mathbb{C}^{R\times 1}$ is the memory vector in the recursion. Associated with a state-space model is the *observability matrix*

$$\mathbf{O}_S = \begin{bmatrix} \mathbf{C} \\ \mathbf{C}\mathbf{A} \\ \vdots \\ \mathbf{C}\mathbf{A}^{S-1} \end{bmatrix} \in \mathbb{C}^{PS\times R}. \tag{5}$$

If the number of block rows S is larger than R it is called the extended observability matrix. Note that if $\mathbf{O}_S$ is the observability matrix of the realization $(\mathbf{A}, \mathbf{C}, \mathbf{x}_0)$ then, $\mathbf{O}_S\mathbf{T}$ is the observability matrix of the realization $(\tilde{\mathbf{A}}, \tilde{\mathbf{C}}, \tilde{\mathbf{x}}_0)$. This implies that the *range space* of the observability matrix is invariant with respect to the realization and is a property of the signal $\mathbf{y}(n)$. The observability matrix $\mathbf{O}_S$ has full rank R if (for all $r = 1, \ldots, R$) the frequencies β_r are distinct, $\omega_r \Delta t$ belong to the interval $(-\pi, \pi)$, $\mathbf{a}_r \neq 0$, and $S \geqslant R$. The result [6] follows by noting that $\mathbf{O}_S$ has a Vandermonde type structure.

2.1. Periodic embedding

A signal $x(n)$ is called N-periodic if $x(n) = x(n + kN)$ for all integers k and $n = 0, \ldots, N-1$. The signal model (2) gives an N-periodic signal $\mathbf{y}(n)$ if and only if $\gamma_r = 0$ and $f_r T$ is an integer, where $r = 1, \ldots, R$ and the total measurement time is denoted by $T = N\Delta t$. For this special case, the DFT coefficients of the signal (i.e., $\mathbf{y}(n)$ for $n = 0, \ldots, N-1$) are the coefficients of the Fourier series expansion of $\mathbf{y}(n)$. This is a desirable property of the DFT and we recover it for an arbitrary signal model (2) by extending the state-space model (4) with an artificial input signal, which creates an observationally identical state-space model which is N-periodic outside the measurement interval $n = 0, \ldots, N-1$. We call this *periodic embedding*, and the modified version of the state-space model is given by

$$\begin{aligned} &\mathbf{x}(n+1) = \mathbf{A}\mathbf{x}(n) + \mathbf{b}u(n), \quad \mathbf{x}(0) = \mathbf{x}_0, \\ &\mathbf{y}(n) = \mathbf{C}\mathbf{x}(n), \end{aligned} \tag{6}$$

where $u(n)$ is defined as

$$u(n) \triangleq \begin{cases} 1 & n = kN - 1, \quad k = 1, 2, \ldots, \\ 0 & \text{otherwise}, \end{cases} \tag{7}$$

which is an N-periodic signal. If $\mathbf{b}$ is chosen as

$$\mathbf{b} \triangleq (\mathbf{I} - \mathbf{A}^N)\mathbf{x}_0 \tag{8}$$

it directly follows that $\mathbf{x}(N) = \mathbf{x}_0$, and all signals in Eqs. (6) are therefore N-periodic. Note that in the measurement interval, the output $\mathbf{y}(n)$ of the modified signal model (6) equals that of the original model (4), and consequently both models are valid for the observed signal. The column vector $\mathbf{b}$ is identically zero when $\mathbf{I} - \mathbf{A}^N = \mathbf{0}$. This happens for the undamped case when the observation interval encompasses exactly an integer number of periods for all sinusoids, and the modification by an input is not necessary to make the signal N-periodic. It is important to note that the periodic embedding is merely a trick enabling a simple derivation of the method. As we will see, it results in a specific term designed to cancel the effect of the original signal *not* being N-periodic. Contrary to what might be thought, we are therefore not introducing any artificial assumptions by adopting the extended model.

2.2. Frequency domain model

The N-point DFT of a signal $\mathbf{x}(n)$ is for $n = 0, \ldots, N-1$ given by

$$\bar{\mathbf{x}}(q) \triangleq \mathrm{DFT}\{\mathbf{x}(n)\}(q) \triangleq \sum_{n=0}^{N-1} \mathbf{x}(n) W_N^{-qn}, \tag{9}$$

where $W_N^q \triangleq \exp(\mathrm{i}2\pi q/N)$ and q denotes the DFT frequency. Consider the modified model (6). Due to the N-periodicity of $\mathbf{x}(n)$ it follows that $\mathbf{x}(N) = \mathbf{x}(0)$ and hence

$$\mathrm{DFT}\{\mathbf{x}(n+1)\}(q) = \sum_{n=0}^{N-1} \mathbf{x}(n+1) W_N^{-qn} = W_N^q \sum_{n=0}^{N-1} \mathbf{x}(n+1) W_N^{-q(n+1)} = W_N^q \bar{\mathbf{x}}(q).$$

The modified signal model (6) can therefore be expressed in the DFT domain as

$$\begin{aligned} W_N^q \bar{\mathbf{x}}(q) &= \mathbf{A}\bar{\mathbf{x}}(q) + \mathbf{b}\bar{u}(q), \\ \bar{\mathbf{y}}(q) &= \mathbf{C}\bar{\mathbf{x}}(q), \end{aligned} \tag{10}$$

where $\bar{\mathbf{y}}(q) \triangleq \mathrm{DFT}\{\mathbf{y}(n)\}(q)$ and $\bar{u}(q) \triangleq \mathrm{DFT}\{u(n)\}(q) = W_N^q$.

3. Estimation algorithm

The derivation of our estimation algorithm starts by forming a vector relation by repeatedly using Eqs. (10). It is easy to show that for the DFT frequency q we have

$$\mathbf{y}_q = \mathbf{O}_S \bar{\mathbf{x}}(q) + \mathbf{G}_S \mathbf{u}_q, \tag{11}$$

where

$$\mathbf{y}_q \triangleq \begin{bmatrix} \bar{\mathbf{y}}(q) \\ W_N^q \bar{\mathbf{y}}(q) \\ W_N^{2q} \bar{\mathbf{y}}(q) \\ \vdots \\ W_N^{(S-1)q} \bar{\mathbf{y}}(q) \end{bmatrix}, \quad \mathbf{u}_q \triangleq \begin{bmatrix} \bar{u}(q) \\ W_N^q \bar{u}(q) \\ W_N^{2q} \bar{u}(q) \\ \vdots \\ W_N^{(S-1)q} \bar{u}(q) \end{bmatrix},$$

and the lower triangular Toeplitz matrix $\mathbf{G}_S$ is

$$\mathbf{G}_S \triangleq \begin{bmatrix} \mathbf{0} & \mathbf{0} & \mathbf{0} & \dots & \mathbf{0} & \mathbf{0} \\ \mathbf{Cb} & \mathbf{0} & \mathbf{0} & \dots & \mathbf{0} & \mathbf{0} \\ \mathbf{CAb} & \mathbf{Cb} & \mathbf{0} & \dots & \mathbf{0} & \mathbf{0} \\ \mathbf{CA}^2\mathbf{b} & \mathbf{CAb} & \mathbf{Cb} & \dots & \mathbf{0} & \mathbf{0} \\ \vdots & \vdots & \vdots & \ddots & \vdots & \vdots \\ \mathbf{CA}^{S-2}\mathbf{b} & \mathbf{CA}^{S-3}\mathbf{b} & \mathbf{CA}^{S-4}\mathbf{b} & \dots & \mathbf{Cb} & \mathbf{0} \end{bmatrix}.$$

Now, assume that a subset of the frequencies on the DFT-grid is selected and denote the M selected frequency indices by $q_1, \dots, q_M$. We will use these M points of the DFT to estimate the sought frequencies. The reason for considering a subset of the DFT data is to provide suppression of interfering signal components residing outside the frequency band of interest, which considerably simplifies the estimation problem. The method works for $2R < M \leqslant N$, where $M = N$ implies that all DFT points are used. The final data matrices are formed by assembling the data vectors as:

$$\mathbf{Y} \triangleq [\, \mathbf{y}_{q_1} \quad \mathbf{y}_{q_2} \quad \cdots \quad \mathbf{y}_{q_M} \,], \tag{12}$$

$$\mathbf{U} \triangleq [\, \mathbf{u}_{q_1} \quad \mathbf{u}_{q_2} \quad \cdots \quad \mathbf{u}_{q_M} \,], \quad \text{and} \tag{13}$$

$$\mathbf{X} \triangleq [\, \bar{\mathbf{x}}(q_1) \quad \bar{\mathbf{x}}(q_2) \quad \cdots \quad \bar{\mathbf{x}}(q_M) \,], \tag{14}$$

and the vector relation (11) is expanded to a matrix one

$$\mathbf{Y} = \mathbf{O}_S\mathbf{X} + \mathbf{G}_S\mathbf{U}. \tag{15}$$

Hence the DFT data in $\mathbf{Y}$ is a sum of two matrix components. The rank of the matrix product $\mathbf{O}_S\mathbf{X}$ equals R, and the second term is the product of the known matrix $\mathbf{U}$ and the unknown matrix $\mathbf{G}_S$. In order to retrieve the frequencies, it suffices to get an estimate of the range space of the extended-observability matrix $\mathbf{O}_S$. The matrix equation (15) has a structure which is well known in the area of subspace based system identification methods [19–21].

3.1. Subspace based method

Starting from the derived identity (15) the identification method consists of the following steps:
(1) Remove the influence of the term $\mathbf{G}_S\mathbf{U}$.
(2) Find a matrix $\mathbf{Z}_S$ which is an estimate of the range space of $\mathbf{O}_S$.
(3) From $\mathbf{Z}_S$ estimate a matrix $\hat{\mathbf{A}}$ which is similar to the original matrix $\mathbf{A}$.
(4) Determine the eigenvalues $\hat{\lambda}_r$ of the matrix $\hat{\mathbf{A}}$ and let the frequency estimates be $\hat{\beta}_r = (\Delta t)^{-1} \log \hat{\lambda}_r$.
(5) Estimate the complex amplitudes $\hat{\mathbf{a}}_r$ of the sinusoids using linear regression.

Each step is now described in more detail.

In subspace methods a standard way to remove the $\mathbf{G}_S\mathbf{U}$ term is by a projection. Define the projection matrix

$$\mathbf{P}^{\perp} \triangleq \mathbf{I} - \mathbf{U}^H(\mathbf{U}\mathbf{U}^H)^{-1}\mathbf{U}, \tag{16}$$

which projects onto the nullspace of $\mathbf{U}$. Here, $\mathbf{U}^H$ denotes the complex conjugate and transpose of $\mathbf{U}$. Applying this projection from right in Eq. (15) results in

$$\mathbf{Y}\mathbf{P}^{\perp} = \mathbf{O}_S\mathbf{X}\mathbf{P}^{\perp}. \tag{17}$$

If $S \leqslant M - R$ it can be shown with a technique similar to [21, Lemma 5] $\operatorname{rank}\{\mathbf{X}\mathbf{P}^{\perp}\} = R$. Hence, $\operatorname{rank}\{\mathbf{Y}\mathbf{P}^{\perp}\} = R$ so the projection matrix does not cancel any part of the range space of $\mathbf{O}_S$.

The range space of $\mathbf{O}_S$ is determined by factoring $\mathbf{Y}\mathbf{P}^{\perp}$ into two rank R matrices. In the noisy case $\mathbf{Y}\mathbf{P}^{\perp}$ will have full rank and we seek for a rank R factorization which is a good approximation. The singular value decomposition (SVD) [22] gives the desired factorization

$$\mathbf{Y}\mathbf{P}^{\perp} = [\,\mathbf{Z}_S \quad \mathbf{Z}_0\,] \begin{bmatrix} \mathbf{S}_S & 0 \\ 0 & \mathbf{S}_0 \end{bmatrix} \begin{bmatrix} \mathbf{V}_S^H \\ \mathbf{V}_0^H \end{bmatrix}, \tag{18}$$

where $\mathbf{S}_S$ denotes the R largest singular values. As an estimate of the range space of the observability matrix $\mathbf{O}_S$ we simply take $\mathbf{Z}_S$ as a basis for the range space. In the noise-free case the range space is exactly recovered since, then, $\mathbf{S}_0$ is zero and $\mathbf{Y}\mathbf{P}^{\perp} = \mathbf{Z}_S\mathbf{S}_S\mathbf{V}_S^H$ so there exists a nonsingular matrix $\mathbf{T}$ such that $\mathbf{Z}_S = \mathbf{O}_S\mathbf{T}$. Consequently $\mathbf{Z}_S$ is an extended-observability matrix for a particular realization of the observed signal $\mathbf{y}(n)$.

The extended-observability matrix (5) has a special block row structure, where each new block-row is the previous block row multiplied by $\mathbf{A}$. Using the shift structure of the observability matrix, a matrix $\hat{\mathbf{A}}$ is determined by minimizing the Frobenius norm (least-squares)

$$\min_{\mathbf{A}} \|\lceil \mathbf{Z}_S \rceil \mathbf{A} - \lfloor \mathbf{Z}_S \rfloor\|_F^2, \tag{19}$$

where $\lceil \mathbf{Z}_S \rceil$ and $\lfloor \mathbf{Z}_S \rfloor$ denotes the $P(S-1)$ first and last rows of $\mathbf{Z}_S$, respectively. The solution is unique since when $S > R$ the matrix $\lceil \mathbf{Z}_S \rceil$ has full rank since $\lceil \mathbf{O}_S \rceil$ has full rank. The fitting problem can alternatively be solved using the total-least-squares (TLS) method [22], which exhibits better threshold properties than does the standard LS method. Finally, the normalized frequency estimates $\hat{\beta}_r\Delta t$ are the logarithm of the eigenvalues of $\hat{\mathbf{A}}$. The method of low rank approximation using the SVD and then using the shift-invariant property of the observability matrix to retrieve $\mathbf{A}$ is known from, e.g. [13,14].

The method has a parameter S called the *auxiliary model order*. It determines the number of block rows in $\mathbf{O}_S$, and must satisfy $R < S \leqslant M - R$. The minimum amount of data needed for a given R is obtained by setting $S = R + 1$, which gives $M_{\min} = 2R + 1$.

Straightforward application of the DFT to $\mathbf{y}(n)$ yields

$$\bar{\mathbf{y}}(q) = \sum_{\substack{r \\ \beta_r\Delta t \neq 2\pi q/N}} \mathbf{a}_r \frac{1 - \mathrm{e}^{\beta_r N\Delta t}}{1 - W_N^{-q}\mathrm{e}^{\beta_r\Delta t}} + \sum_{\substack{r \\ \beta_r\Delta t = 2\pi q/N}} \mathbf{a}_r N. \tag{20}$$

Hence, $\bar{\mathbf{y}}(q)$ is a linear function of the complex amplitudes $\mathbf{a}_r$ when β_r are known (or estimated as above). Therefore, $\hat{\mathbf{a}}_r$ can be estimated by linear regression as a final step.

3.2. Real-valued signals

The case when $\mathbf{y}(n)$ is a real-valued signal is included in the signal model (2). The model order R is then twice the number of real sinusoids and the frequencies and amplitudes are pairwise complex conjugated, i.e., $\beta_r = \beta_{r+1}^*$ and $\mathbf{a}_r = \mathbf{a}_{r+1}^*$ for r odd. When $\mathbf{y}(n)$ is real there also exists state-space realizations of the signal with only real-valued matrices. This implies that the extended-observability space can be represented by a real-valued matrix. The method can be modified to impose the real-valued signal constraint by only estimating a real-valued observability matrix and is accomplished by calculating the SVD of the real matrix (similar to [23])

$$[\,\operatorname{Re}\mathbf{Y}\mathbf{P}^{\perp} \quad \operatorname{Im}\mathbf{Y}\mathbf{P}^{\perp}\,] = \mathbf{O}_S[\,\operatorname{Re}\mathbf{X}\mathbf{P}^{\perp} \quad \operatorname{Im}\mathbf{X}\mathbf{P}^{\perp}\,]. \tag{21}$$

This leads to a real-valued $\hat{\mathbf{A}}$ which has complex conjugated eigenvalues, and hence the estimated frequencies will be pairwise complex conjugated as desired. Since the number of columns are doubled in Eq. (21), the valid interval for the auxiliary model order becomes $R < S \leqslant 2M - R$. Note that in the real valued case the DFT coefficients corresponding to negative frequencies gives no additional information since $\bar{\mathbf{y}}(q) = \bar{\mathbf{y}}^*(N - q)$.

3.3. Reduction of disturbances

A measured signal will to some extent always be subject to disturbances. Commonly we model such disturbances as additive random signals. The presented method suppresses the influence of disturbances in two ways. First, the DFT provides an averaging of the random disturbances which leads to a reduction of the variance if $M < N$. The frequency domain filtering, by only using a subset of the DFT coefficients, also suppresses disturbances with spectral energy residing outside the selected frequency interval. A second reduction is also obtained by the SVD factorization where a full rank matrix $\mathbf{YP}^{\perp}$ is approximated by a rank R one.

In the lossless case when $\beta_r = \mathrm{i}\omega_r$ for $r = 1, \ldots, R$, the sinusoidal signal can be time reversed and complex conjugated and still be described by the same basic model of the same order. Hence, we can artificially double the number of observations by considering the backward signal as an additional vector observation. Combining the forward and backward signals is a well known method for the frequency estimation problem [5], as it often improves the estimation accuracy. Assume the signal $\mathbf{y}(n)$ in Eq. (1) is observed for $n = 0, \ldots, N - 1$, and define a new backward signal which is the time reversed conjugate of $\mathbf{y}(n)$. By joining the forward and backward signals

$$\mathbf{y}_{\mathrm{fb}}(n) \triangleq \begin{bmatrix} \mathbf{y}(n) \\ \mathbf{y}^*(N-1-n) \end{bmatrix}, \quad n = 0, \ldots, N-1, \tag{22}$$

it is easy to show that

$$\mathbf{y}_{\mathrm{fb}}(n) = \sum_{r=1}^{R} \begin{bmatrix} \mathbf{a}_r \\ \mathbf{a}_r^* \mathrm{e}^{-\mathrm{i}\omega_r (N-1)\Delta t} \end{bmatrix} \mathrm{e}^{\mathrm{i}\omega_r n \Delta t}. \tag{23}$$

Note that the compound forward–backward signal $\mathbf{y}_{\mathrm{fb}}(n)$ is still described with R complex sinusoids. Since the forward–backward signal is a sum of vector-valued sinusoids the method presented above directly applies.

4. Numerical results

We test the frequency domain subspace algorithm in three different settings. In the first test case, we use the FDTD scheme to solve for the electromagnetic fields in a brick shaped cavity and we investigate the estimation of eigenfrequencies for both lossless and lossy homogeneous materials inside the cavity. As a second test case, we consider the FEM applied to a lossless three-dimensional bow-tie microwave resonator, which is discretized by an unstructured grid of tetrahedrons. For the final test case, we use the FDTD scheme for a free-space computation which involves a brick shaped metal cavity with an aperture and estimate the resonant frequencies and quality factors for the lowest modes. The tests are for real-valued signals and we estimate $\hat{\mathbf{A}}$ by the least-squares method as shown in Eq. (19).

4.1. Test 1 – Brick shaped cavity

The first test case is a brick shaped cavity with perfect electric conductor (PEC) walls. We place one corner of the cavity at the origin and align the edges of the cavity with the positive axes of a Cartesian

coordinate system. The sides of the cavity are $l_x = 11$ mm, $l_y = 13$ mm and $l_z = 17$ mm along the x-, y- and z-axis, respectively. The interior of the cavity is characterized by a homogeneous medium with $\epsilon_r = \mu_r = 1$ and the conductivity $\sigma \geqslant 0$. We exploit the FDTD scheme to solve for the electromagnetic fields inside the cavity which is discretized by cubes of side h. The time step is set to the Courant limit $\Delta t = h/\sqrt{3}c_0$, where c_0 is the speed of light.

Given the difference equations of the FDTD scheme applied to the brick cavity with PEC walls, there are analytical expressions for the *numerical* eigenfrequencies and eigenmodes. Consequently, we can construct an initial condition by forming a linear combination of the eigenmodes with prescribed magnitude and phase. Clearly, this will not be feasible for a general case but it allows us to fully control the spectrum of the solution which is useful for testing. The analytical expression for the numerical eigenfrequencies ω in the lossless case ($\sigma = 0$) is given by

$$\left[\frac{h}{c_0\Delta t}\sin\left(\frac{\omega\Delta t}{2}\right)\right]^2 = \sin^2\left(\frac{k_x h}{2}\right) + \sin^2\left(\frac{k_y h}{2}\right) + \sin^2\left(\frac{k_z h}{2}\right), \tag{24}$$

where $k_x = \pi n_x/l_x$, $k_y = \pi n_y/l_y$ and $k_z = \pi n_z/l_z$, with appropriate integer values for n_x, n_y and n_z. For the lossy case $\sigma > 0$, the numerical eigenfrequencies $\beta = -\gamma + \mathrm{i}\omega$ satisfy

$$\exp(\beta\Delta t) = \frac{\xi^2 - \kappa^2 \pm \mathrm{i}\sqrt{\kappa^2(2\xi^2 - \kappa^2) - \zeta^2}}{\xi^2 + \zeta}, \tag{25}$$

where $\kappa^2 = 4h^{-2}[\sin^2(k_x h/2) + \sin^2(k_y h/2) + \sin^2(k_z h/2)]$, $\xi^2 = 2\mu_0\epsilon_0/\Delta t^2$ and $\zeta = \mu_0\sigma/\Delta t$.

In the tests for the brick shaped cavity, we choose to record the signal

$$\mathbf{y}(n) = \begin{bmatrix} \hat{x}\cdot\vec{E}(\vec{r}_0 + h/2\hat{x}, n) \\ \hat{y}\cdot\vec{E}(\vec{r}_0 + h/2\hat{y}, n) \\ \hat{z}\cdot\vec{E}(\vec{r}_0 + h/2\hat{z}, n) \end{bmatrix}, \tag{26}$$

where $\vec{r}_0 = (3h, 5h, 7h)$ and $\hat{x}$ is the unit vector along the x-axis, etc.

4.1.1. Excitation by initial conditions

We construct an initial condition for the FDTD computation by setting the magnitudes to unity and the phases to random numbers for the modes with the $R/2$ lowest eigenfrequencies, where R is an even integer. The magnitudes of the remaining modes are set to zero. Thus, the model order R is equal to twice the number of excited modes and we use all DFT points for the estimation, i.e., $M = N$.

For this setting, we compute the relative error from $e_r = |\hat{\omega}_r - \omega_r|/|\omega_r|$ and study its maximum value $e_{\max} = \max_r e_r$ as a function of the number of time steps N used by the frequency domain subspace algorithm. Fig. 1 shows $e_{\max}$ computed from the compound forward–backward signal $\mathbf{y}_{\mathrm{fb}}(n)$, which is constructed according to Eq. (22). The dashed curves indicate $S = S_{\min} = R + 1$ while solid curves are based on $S = 2S_{\min}$ for the four cases: (a) $R/2 = 10$ (□), (b) $R/2 = 20$ (△), (c) $R/2 = 40$ (◇) and (d) $R/2 = 80$ (▽), where these symbols carry the information about $R/2$ throughout this section.

Next, we study the case when only the forward signal $\mathbf{y}(n)$ is used and the corresponding results are shown in Fig. 2, where dashed curves are computed with $S = S_{\min}$ and solid curves with $S = 4S_{\min}$. The combination $S = S_{\min}$ and $R/2 = 80$ is not shown in Fig. 2 since the maximum relative error is roughly unity for $N \leqslant 7500$. Note that $\mathbf{y}(n)$ with a higher auxiliary model order S can give roughly the same accuracy in the estimated frequencies as the forward–backward signal $\mathbf{y}_{\mathrm{fb}}(n)$ with a lower S.

For the results presented in Figs. 1 and 2, we used the FDTD cell size $h = 1$ mm and computed ω_r from Eq. (24). As compared to the physical eigenfrequencies, which are recovered when $h \to 0$, the

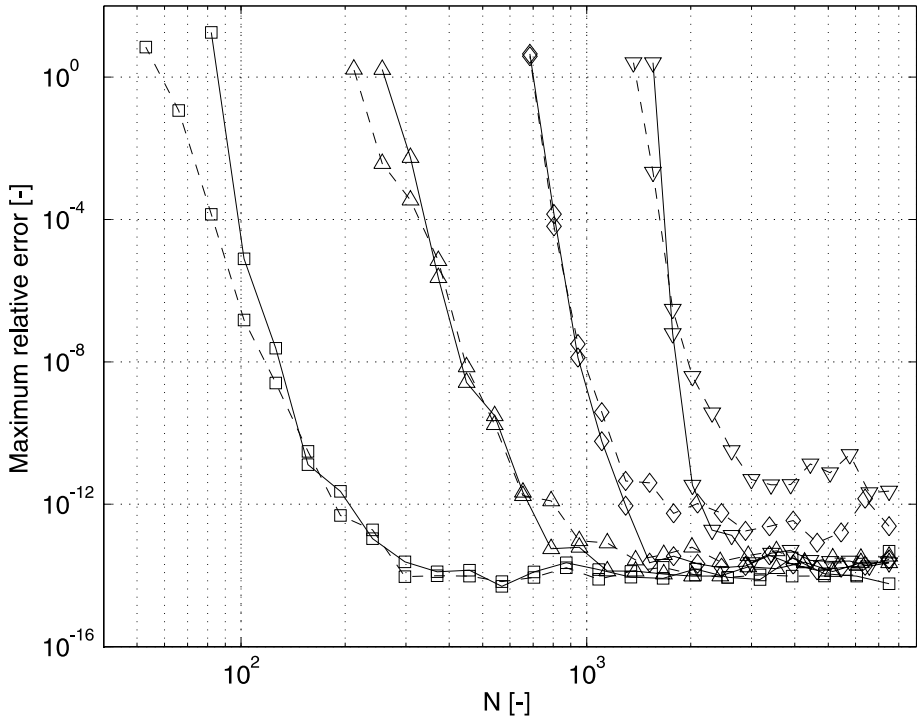

Fig. 1. The maximum relative error $\max_r |\hat{\omega}_r - \omega_r|/|\omega_r|$ given the joined forward–backward signal $\mathbf{y}_{\text{fb}}(n)$ when $S = S_{\min} = R + 1$ (dashed curves) and $S = 2S_{\min}$ (solid curves) for: (a) $R/2 = 10$ (□), (b) $R/2 = 20$ (△), (c) $R/2 = 40$ (◇), and (d) $R/2 = 80$ (▽).

relative error in ω_r when $h = 1$ mm is in the interval from 0.02% to 2.5% for the lowest 80 eigenfrequencies of the brick cavity. An error of a couple of percent is acceptable for many engineering applications. We conclude that, for $\sigma = 0$, the error introduced by the frequency domain subspace algorithm can be made negligible as compared to the discretization error of the FDTD scheme. Moreover, the accuracy in the estimates is satisfactory for extrapolation of the eigenfrequencies to zero cell size as well as when the frequency domain subspace algorithm is applied to sampled data computed by higher order finite difference or finite element schemes. In fact, the frequency domain subspace algorithm in conjunction with an infinite precision computer would yield exact frequency estimates $\hat{\omega}_r = \omega_r$. The results shown in Figs. 1 and 2 are, thus, a consequence of the estimation performed with 16 digits of precision.

Next, we investigate the lossy case $\sigma > 0$ where, as previously discussed, we can only use the forward signal for the frequency estimation. Fig. 3 shows the maximum relative error (based on $e_r = |\hat{\beta}_r - \beta_r|/|\beta_r|$) when $S = 4S_{\min}$. Solid, dashed and dash-dotted curves indicate the results when $\sigma = 0.01$, $\sigma = 0.1$ and $\sigma = 1$, respectively. We find that $e_{\max}$ as a function of the number of time steps does not change significantly for $\sigma < 0.01$, as compared to the results achieved for $\sigma = 0.01$. We define the quality factor as

$$Q_r \triangleq \frac{\sqrt{\gamma_r^2 + \omega_r^2}}{2\gamma_r} \tag{27}$$

for the rth resonance. We have $8 < Q_r < 30$ when $\sigma = 0.1$ for the lowest 80 eigenmodes of the cavity and, similarly, $80 < Q_r < 300$ when $\sigma = 0.01$. In the current setting with $\sigma = 1$, we cannot compute accurate estimates for the frequencies when $R/2 = 20$, 40 or 80 but for the case $R/2 = 10$ (with $0.8 < Q_r < 1.6$) we can achieve $e_{\max} < 10^{-6}$.

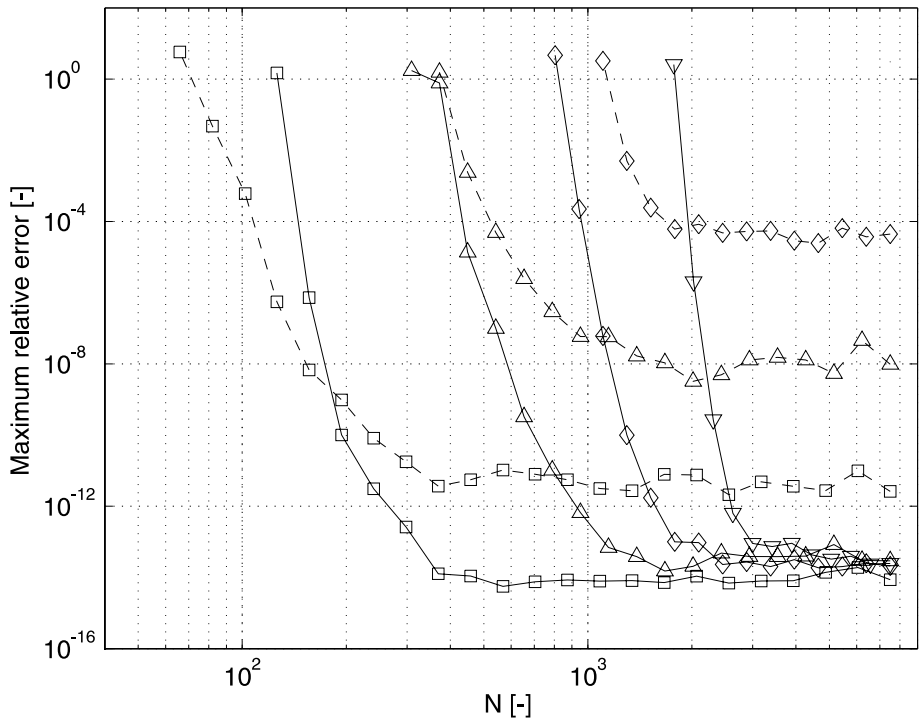

Fig. 2. The maximum relative error $\max_r |\hat{\omega}_r - \omega_r|/|\omega_r|$ given only the forward signal $\mathbf{y}(n)$ when $S = S_{\min} = R + 1$ (dashed curves) and $S = 4S_{\min}$ (solid curves) for: (a) $R/2 = 10$ (□), (b) $R/2 = 20$ (△), (c) $R/2 = 40$ (◇), and (d) $R/2 = 80$ (▽).

The brick shaped cavity supports a number of eigenmodes with degenerated eigenfrequencies. The corresponding numerical eigenfrequencies, computed by the FDTD scheme employed here, are also degenerated. Each numerically degenerated eigenfrequency appear only once among the estimates since a unique signal model (2) requires that the frequencies β_r are distinct. Physically degenerated eigenfrequencies might get separated in the numerical solution of the problem, e.g., when the FEM uses an unstructured grid.

The frequency domain subspace algorithm can be interpreted as a frequency domain version of the well known ESPRIT [14] and the two methods are closely related for the case when the frequency domain subspace algorithm uses all the DFT points for the estimation, which is the case for the tests above. This is confirmed by additional tests where the standard ESPRIT is applied to the previous test cases and, almost identically, reproduced the results shown in Figs. 1–3. However, the frequency domain subspace algorithm can also work with a subset of DFT points in a preselected sub-band, which allows for suppression of out-of-band disturbances and reduction of the computational cost. We explore this feature after a discussion on the temporal dependence of the excitation.

4.1.2. Excitation by time dependent sources

For most applications of interest, the numerical eigenfrequencies and eigenmodes are not known a priori. We can treat such a situation by exciting the system with a boundary condition or a source current which is the product of some fixed spatially dependent function and an amplitude with a specified time dependence. Specifically for the brick cavity, we use the amplitude $I(n)$ for the current along the edges

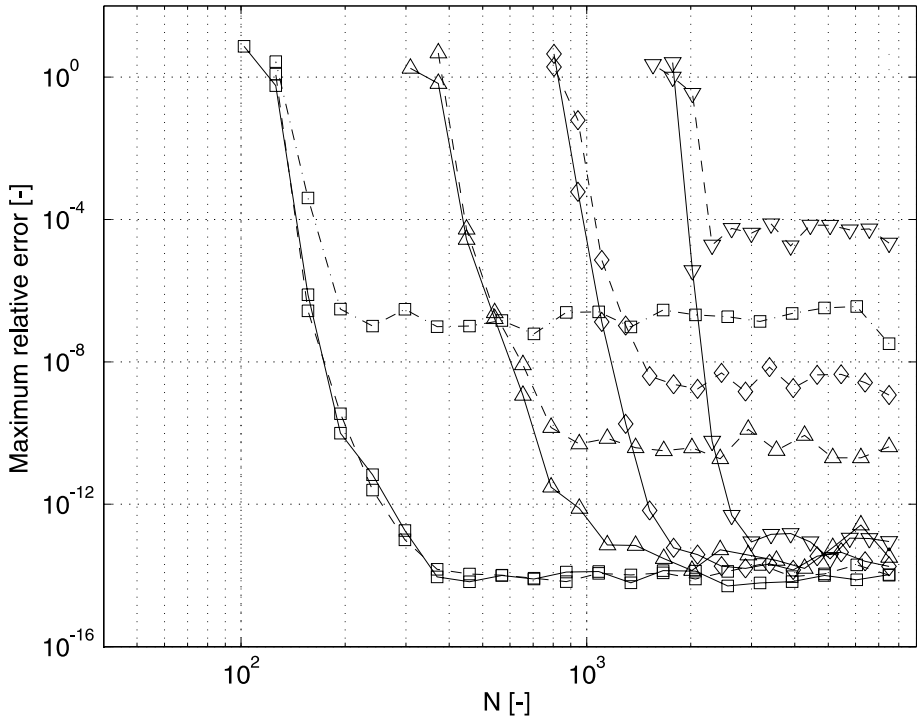

Fig. 3. The maximum relative error $\max_r |\hat{\beta}_r - \beta_r|/|\beta_r|$ given the forward signal $\mathbf{y}(n)$ and $S = 4S_{\min} = 4(R+1)$ when $\sigma = 0.01$ (solid curves), $\sigma = 0.1$ (dashed curves) and $\sigma = 1$ (dash-dotted curve) for: (a) $R/2 = 10$ (□), (b) $R/2 = 20$ (△), (c) $R/2 = 40$ (◇), and (d) $R/2 = 80$ (▽).

forming the closed loop shown in Fig. 4. This kind of current loop ensures that the electrostatic solutions $\vec{E} = -\nabla\phi$, which are supported by the FDTD scheme, are not excited.

A sinusoidal which is amplitude modulated with a Gaussian is a popular choice for time varying excitations in electromagnetic computations. This gives a signal which is optimal in the sense that the mean-square sense time-bandwidth product is the smallest possible [24]. For the proposed frequency domain subspace algorithm, however, it is desirable to create a time dependent excitation such that its frequency spectrum has a unity magnitude in the frequency band of interest and a zero magnitude outside this band. Clearly, it is of general interest in time domain computations to use sources which only excite the frequency band where the response is sought.

Relatively short time domain signals with a favorable spectrum can be constructed by exploiting the well-established digital filter design technology developed for signal processing. The impulse response of the filter is then used for the time dependence $I(n)$ of the excitation, i.e., we set $I(n) = \mathscr{F}(\delta(n))$ where $\mathscr{F}$ denotes the filter and $\delta(n)$ is the discrete-time unit impulse function ($\delta(0) = 1$ and $\delta(n) = 0$ for $n > 0$). For a computation of the lowest eigenfrequencies, we wish to design a low-pass filter with steep roll off and large attenuation in the stop-band. We denote the pass-band and stop-band edge frequencies by f_p and f_s, respectively, and the corresponding peak ripple values by δ_p and δ_s. In the following, we use `remezord` and `remez` implemented in `MATLAB` to design lowpass filters with $\delta_p = 0.1$ and $\delta_s = 10^{-8}$. The pass-band and stop-band magnitudes are set to unity and zero, respectively. The roll off and stop-band ripple of a low order filter can efficiently be improved by using the impulse response of the filter as the input to the filter itself, i.e., we set $I(n) = \mathscr{F}(\mathscr{F}(\delta(n)))$. Obviously, this "refiltering" can be exploited several times but with

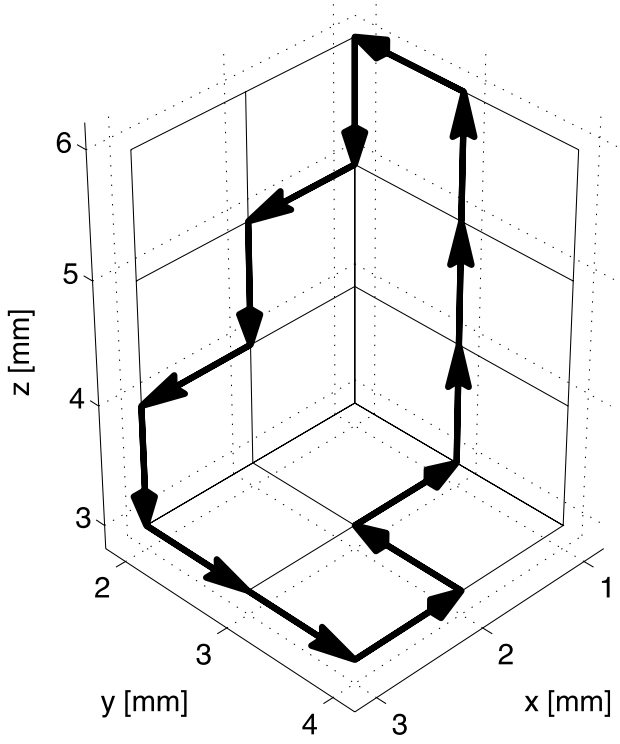

Fig. 4. The current loop exciting the FDTD computation for the cell size $h = 1$ mm. The cavity has one corner at origin and its edges are aligned with the positive x-, y- and z-axes.

the cost of increasing the length of the time domain excitation signal and the pass-band ripple δ_p. One refiltering gives a stop-band with the amplitude response $\delta_s^2 = 10^{-16}$ which is essentially zero as compared to the close to unity pass-band response when using a computer with 16 digits of precision.

4.1.3. Determination of the model order

In Section 4.1.1, we set the model order equal to twice the number of eigenfrequencies based on the precise knowledge of the solution. For realistic applications, however, the number of eigenfrequencies which reside in a preselected frequency band is a priori unknown and the model order R must be determined. In many cases, a rough estimate of R can be found, e.g., by using a simplified model of the electromagnetic system. Equipped with such an estimate, an appropriate combination of the auxiliary model order S and the number of time steps N can be chosen from Figs. 1–3 or similar information. After the data $\mathbf{y}(n)$ have been sampled from the electromagnetic computation, we use the frequency domain subspace algorithm with the selected DFT points and auxiliary model order S to compute the singular values in Eq. (18). The singular values appear in pairs, i.e., one pair for each real-valued sinusoid, and ideally they separate into two distinct groups: (A) large singular values which correspond to sinusoids with large energy and (B) small singular values which represent the disturbances $\mathbf{w}(n)$. Given an appropriate selection of the involved parameters, the two groups are separated by a significant gap and we set the model order R equal to the number of large singular values associated with group A.

This procedure to determine the model order is demonstrated for the lossless brick cavity excited by the current loop shown in Fig. 4. The time dependence of the current is based on a lowpass filter with

$f_p\Delta t = 0.048$ and $f_s\Delta t = 0.053$. This choice of f_p and f_s will excite the nine lowest eigenfrequencies and we search for these eigenfrequencies in the frequency band $0 < f\Delta t \leqslant 0.1$. We record the signal $\mathbf{y}(n)$ during $N = 400$ time steps (which gives $M = 39$) and exploit the compound forward–backward signal $\mathbf{y}_{fb}(n)$ for the frequency estimation. The spectrum of the excitation $|\bar{I}(q)|$ is shown in Fig. 5 by the dashed line and the response $|\bar{\mathbf{y}}(q)|$ is shown by the solid line with circles indicating the DFT frequencies. It should be noted that the spectrum of the undamped sinusoidal response is computed from a time domain signal with only $N = 400$ samples and that this signal is not N-periodic. Therefore, the response suffers from a considerable amount of spectral leakage, which is clearly displayed in Fig. 5. On the other hand, the spectrum of the excitation signal is computed from all of its non-zero values, which gives a spectrum without leakage. The lowest eigenfrequencies computed from Eq. (24) are indicated by the dotted vertical lines in Fig. 5 and, obviously, only the modes in the frequency band $0 < f\Delta t < f_s\Delta t$ are excited.

We apply the frequency domain subspace algorithm to $\mathbf{y}(n)$ and study the singular values of Eq. (18). Here, we test all feasible values for the auxiliary model order S, i.e., $S = 2, \ldots, 2M - 1$ where $M = 39$, in order to study the sensitivity of the singular values with respect to S. Note that the total number of singular values given from Eq. (18) depends on S, and we get at least two and at most 66 singular values. The computed singular values fall on the vertical lines in-between the terminating triangles shown in Fig. 6, where (for each individual S) the singular values are sorted in descending order and labeled consecutively with integer indices starting from one. The singular values computed for $S = 19$ are indicated by horizontal lines in Fig. 6. We note that the singular values are rather insensitive to the selected auxiliary model order S. The first group A consists of large singular values which correspond to sinusoids with large energy in the preselected frequency band and, consequently, we set the model order R equal to the number of singular values in group A, i.e., $R/2 = 9$.

The size of the gap which separates the two groups of singular values can be controlled by the transition region in-between the pass- and stop-band of the filter used for the time dependence of the excitation. Provided that the spatial configuration of the excitation couples well to the eigenmodes of interest, a

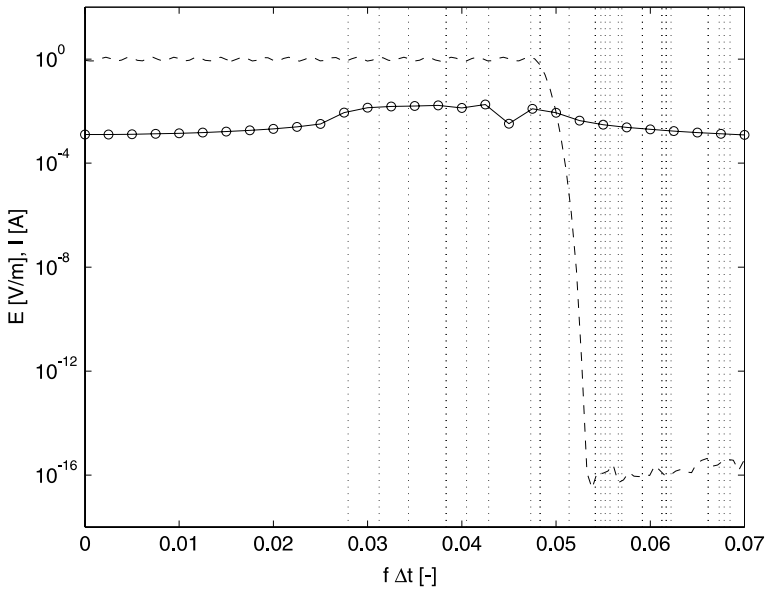

Fig. 5. The excitation and response for the brick cavity: dashed line – magnitude of the DFT for the excitation $I(n)$, solid line with circles – magnitude of the DFT for the response $\mathbf{y}(n)$ and dotted vertical lines – eigenfrequencies given from Eq. (24).

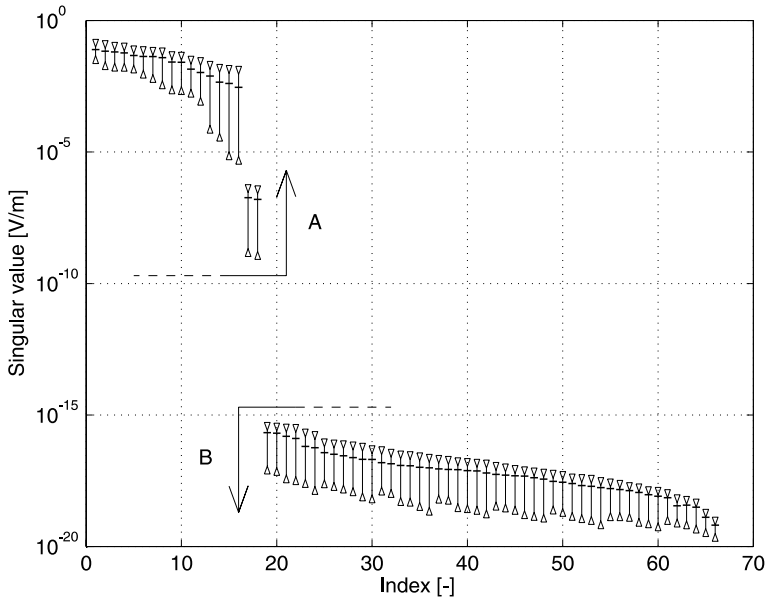

Fig. 6. The computed singular values for $S = 2, \ldots, 2M - 1$ fall on the bars shown by the vertical lines terminated by triangles. For each S, the singular values are sorted in descending order and labeled consecutively with integer indices starting from one. The singular values computed for $S = 19$ are indicated by horizontal lines.

transition region (f_p, f_s) occupied by eigenfrequencies f_r implies that the corresponding eigenmodes will be gradually less excited as their eigenfrequencies are located closer to the stop-band. Correspondingly, the gap which separates the two groups of singular values will be less pronounced. This is less of a problem in practice, however, since the spectrum of the excitation is known and this information can be used to interpret the estimated frequencies together with their amplitudes.

The excitation used for Figs. 5 and 6 has a duration of 1802 time steps. In fact, the number of time steps used for the excitation can be reduced considerably without loosing the possibility to estimate the model order R from the singular values. Therefore, we lower the pass-band edge frequency to $f_p \Delta t = 0.038$, which gives an excitation with the duration of 602 time steps. The remaining parameters in the above setting are kept and we use $S = 19$.

For this new excitation, we investigate the estimated eigenfrequencies for the model orders $R/2 =$ 8, 9, 10 and 11. For the model order $R/2 = 9$, Table 1 shows the values for $\|\hat{\mathbf{a}}_r\| = (\hat{\mathbf{a}}_r^H \hat{\mathbf{a}}_r)^{1/2}$ and $\hat{f}_r \Delta t$

Table 1
The estimated amplitudes and frequencies for $R/2 = 9$ together with the relative error in the estimated frequencies

$\|\hat{\mathbf{a}}_r\|$	$\hat{f}_r \Delta t$	$\lvert\hat{f}_r - f_r\rvert / \lvert f_r\rvert$
1.4880×10^{-5}	0.0279327	5.5×10^{-15}
2.3219×10^{-5}	0.0312200	9.2×10^{-15}
1.6033×10^{-5}	0.0343410	5.9×10^{-15}
1.2256×10^{-5}	0.0383322	3.3×10^{-15}
2.0656×10^{-6}	0.0404952	1.6×10^{-14}
1.1496×10^{-6}	0.0428419	1.2×10^{-14}
7.5826×10^{-11}	0.0473102	1.1×10^{-10}
1.6427×10^{-10}	0.0483003	5.2×10^{-11}
8.7975×10^{-15}	0.0513926	7.1×10^{-7}

Table 2
The estimated amplitudes and frequencies for $R/2 = 8$, 10 and 11

$R/2 = 8$		$R/2 = 10$		$R/2 = 11$	
$\|\hat{\mathbf{a}}_r\|$	$\hat{f}_r\Delta t$	$\|\hat{\mathbf{a}}_r\|$	$\hat{f}_r\Delta t$	$\|\hat{\mathbf{a}}_r\|$	$\hat{f}_r\Delta t$
1.4880×10^{-5}	0.0279327	1.4880×10^{-5}	0.0279327	1.4880×10^{-5}	0.0279327
2.3219×10^{-5}	0.0312200	2.3219×10^{-5}	0.0312200	2.3219×10^{-5}	0.0312200
1.6033×10^{-5}	0.0343410	1.6033×10^{-5}	0.0343410	1.6033×10^{-5}	0.0343410
1.2256×10^{-5}	0.0383322	1.2256×10^{-5}	0.0383322	1.2256×10^{-5}	0.0383322
2.0656×10^{-6}	0.0404952	2.0656×10^{-6}	0.0404952	2.0656×10^{-6}	0.0404952
1.1496×10^{-6}	0.0428419	1.1496×10^{-6}	0.0428419	1.1496×10^{-6}	0.0428419
7.5831×10^{-11}	0.0473103	7.5826×10^{-11}	0.0473102	7.5826×10^{-11}	0.0473102
1.6425×10^{-10}	0.0483005	1.6427×10^{-10}	0.0483003	1.6427×10^{-10}	0.0483003
–	–	8.7974×10^{-15}	0.0513926	8.7974×10^{-15}	0.0513925
–	–	2.0393×10^{-19}	0.0881328	2.4425×10^{-19}	0.0860387
–	–	–	–	2.9695×10^{-19}	0.0879041

together with the relative error in the estimated eigenfrequencies, where the estimates $\hat{\mathbf{a}}_r$ are computed by linear regression. It is noticed that the frequency estimates are less accurate for sinusoids with smaller amplitudes, i.e., those residing in the transition region in-between the pass- and stop-band.

Table 2 shows the corresponding values $\|\hat{\mathbf{a}}_r\|$ and $\hat{f}_r\Delta t$ when the model order is $R/2 = 8$, 10 and 11. We find that, as $R/2$ is incremented from 10 to 11, the tenth eigenfrequency (which has a very small amplitude) changes while the first nine eigenfrequencies take the same values as shown in Table 1. This is a strong distinguishing feature that the correct model order is $R/2 = 9$.

4.2. Test 2 – Three-dimensional bow-tie microwave resonator

As a second test case, we consider the three-dimensional bow-tie microwave resonator shown in Fig. 7, where the PEC walls of the cavity are discretized by triangles. The cavity region is based on the cube which occupies the volume $|x| < 100$ mm, $|y| < 100$ mm and $|z| < 100$ mm. From this cube, we remove the volume inside two spheres with radii $R_x = 200$ mm centered along the x-axis at $x = \pm 250$ mm. Similarly, we remove the volume inside the spheres with radii $R_y = 250$ mm centered along the y-axis at $y = \pm 300$ mm and the spheres with radii $R_z = 300$ mm centered along the z-axis at $z = \pm 350$ mm. The cavity is discretized by unstructured tetrahedrons with the average edge length $h \simeq 6.3$ mm.

For this discretization, we apply Galerkin's method to Maxwell's equations

$$\nabla \times \nabla \times \vec{E}(\vec{r}, t) + c_0^{-2}\partial_t^2 \vec{E}(\vec{r}, t) = -\mu_0 \partial_t \vec{J}(\vec{r}, t), \quad \vec{r} \in \Omega,$$

$$\hat{n} \times \vec{E}(\vec{r}, t) = \vec{0}, \quad \vec{r} \in \partial\Omega,$$

where $\partial\Omega$ is the boundary of the computational domain Ω. The spectrum of the solution $\vec{E}(\vec{r}, t)$ is controlled by the time dependence of $\partial_t \vec{J}(\vec{r}, t)$. We use the linear edge elements of Nédélec [25], which gives a system of coupled ordinary differential equations (ODE) $\mathbf{S}\mathbf{e}(t) + c_0^{-2}\mathbf{M}\partial_t^2\mathbf{e}(t) = \mathbf{f}(t)$, where $\mathbf{e}(t) = [E_1(t), E_2(t), \ldots, E_J(t)]^{\mathrm{T}}$. The electric field along the interior edge j is denoted $E_j(t)$, where $j = 1, 2, \ldots, J$ and J is the total number of interior edges. Here, the positive semi-definite "stiffness"-matrix $\mathbf{S} \in \mathbb{R}^{J \times J}$ represents the $\nabla \times \nabla \times$-operator and the positive definite "mass"-matrix $\mathbf{M} \in \mathbb{R}^{J \times J}$ represents the identity operator. The autonomous system of ODEs is integrated in time by the non-dissipative Newmark scheme [26]

$$[\mathbf{M} + (c_0\Delta t)^2\theta\mathbf{S}]\mathbf{e}(n+1) = [2\mathbf{M} + (c_0\Delta t)^2(2\theta - 1)\mathbf{S}]\mathbf{e}(n) - [\mathbf{M} + (c_0\Delta t)^2\theta\mathbf{S}]\mathbf{e}(n-1), \tag{28}$$

where θ controls the implicitness and $\theta \geqslant 1/4$ guarantees stability for all time steps. We set $\theta = 1/4$ and use the time step $\Delta t = h/c_0$. The PETSc-package [27] is employed to solve the sparse system of linear equations

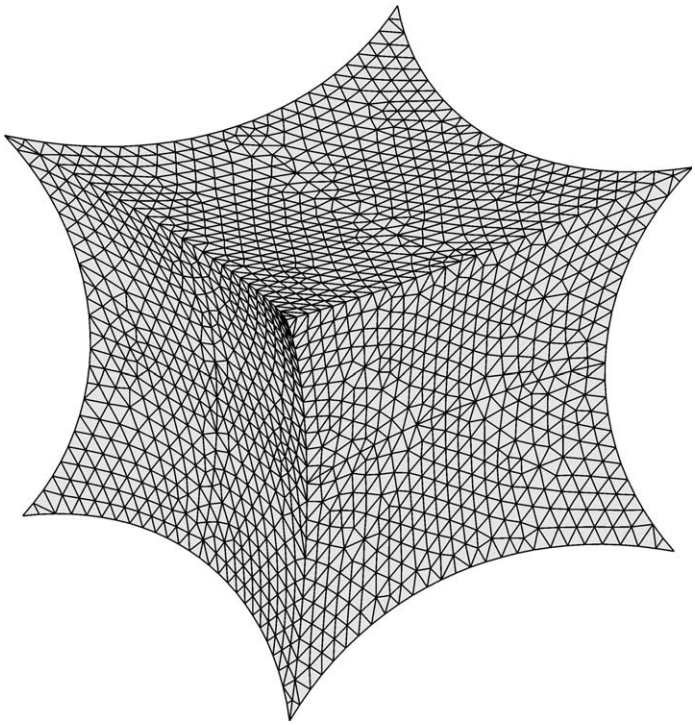

Fig. 7. Surface discretization of three-dimensional bow-tie microwave resonator.

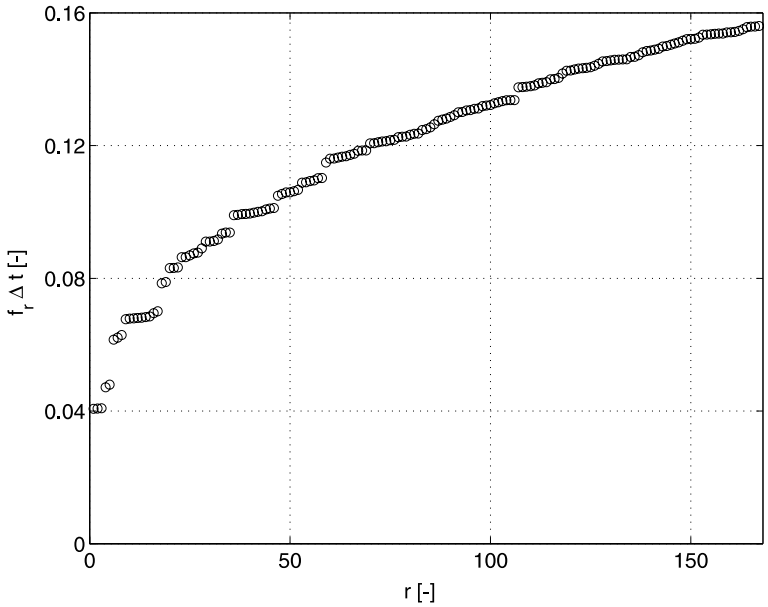

Fig. 8. The first 167 eigenfrequencies for the three-dimensional bow-tie microwave resonator.

(28) by the conjugate gradient method with a zero fill-in incomplete Cholesky preconditioner. We used a relative decrease of 10^{-12} in the residual norm as the termination criterion for the iterative solver, which resulted in roughly 25 iterations per time step.

We exploit the frequency domain subspace algorithm to estimate the 167 lowest resonant frequencies supported by the three-dimensional bow-tie microwave resonator. The estimated resonant frequencies are shown in Fig. 8, where we have used the following procedure to eliminate the discretization error due to the time integration scheme (28). Consider the rth eigenmode $\tilde{\mathbf{e}}_r$ of Eq. (28) with the growth factor $\hat{\rho}_r = \exp(\mathrm{i}2\pi\hat{f}_r^{\mathrm{TD}}\Delta t)$, where $\hat{f}_r^{\mathrm{TD}}$ is estimated by the frequency domain subspace algorithm. For this mode, the time integration scheme (28) can be reduced to $\mathbf{S}\tilde{\mathbf{e}}_r = (2\pi\hat{f}_r^{\mathrm{FD}}/c_0)^2\mathbf{M}\tilde{\mathbf{e}}_r$, where $\hat{f}_r^{\mathrm{FD}}\Delta t = \pm\mathrm{i}(\hat{\rho}_r - 1)/(2\pi\sqrt{\theta\hat{\rho}_r^2 - (2\theta-1)\hat{\rho}_r + \theta})$ is the eigenfrequency of the eigenvalue problem formulated in frequency domain. Consequently, $\hat{f}_r^{\mathrm{FD}}$ does not suffer from numerical errors due the time integration in Eq. (28). For comparison, we also computed the reference values f_r^{EP} by explicitly solving the frequency domain eigenvalue problem. The deviation $|\hat{f}_r^{\mathrm{FD}} - f_r^{\mathrm{EP}}|/|f_r^{\mathrm{EP}}|$ is found to be less than 10^{-7} for all the estimated frequencies. We used `ARPACK` [28] to solve the eigenvalue problem which has almost 48,000 degrees of freedom.

It is difficult to estimate all 167 frequencies concurrently and therefore we use the following technique to achieve accurate estimates with a relatively small computational cost. We partition the frequency band of interest into a sequence of five sub-bands $(f_\mathrm{l}, f_\mathrm{u})$ as shown in Table 3. The temporal part of the excitation for each individual sub-band is based on a filter with a unity response within the sub-band and a null response otherwise, as discussed in Section 4.1.2. The filters overlap each other somewhat so that all resonances can safely be detected. The computer time required for the FEM computation is, in general, many orders of magnitude larger than the time needed for the estimation of the sought frequencies. Therefore, we perform one FEM computation where the sub-bands A, C and E are excited simultaneously. The resonant frequencies in the sub-band `A` can then be estimated to a high accuracy by using only the DFT points which are residing within A and, thus, the out-of-band signals in C and E are effectively suppressed. We achieve very high accuracy for the frequency estimates provided that the out-of-band disturbances are not too close to the DFT points selected for the estimation. Similarly, we estimate the frequencies in C and E without any additional FEM computations. Next, we perform a new FEM computation where the sub-bands B and D are excited simultaneously and, similarly, the resonant frequencies are estimated for B and D separately. Table 3 summarizes the parameters used for the frequency domain subspace algorithm applied to the compound forward–backward signal $\mathbf{y}_{\mathrm{fb}}(n)$, which was constructed from ten unknowns randomly chosen from the FEM solution $\mathbf{e}(n)$.

The computed spectrum for the bow-tie microwave resonator contains some very closely spaced eigenfrequencies. The smallest separation in frequency of two adjacent resonances is $9.2 \times 10^{-7}/\Delta t$. Consequently, 2.2×10^6 time steps are needed to get three DFT points in-between these two resonant frequencies. The frequency domain subspace algorithm needs 23,000 time steps in total for the two FEM computations, which includes the time steps used for the excitation. Thus, the frequency domain subspace algorithm

Table 3
The frequency band $0 < f\Delta t < 0.1460$ is divided into five sub-bands $(f_\mathrm{l}, f_\mathrm{u})$

Band	$f_\mathrm{l}\Delta t$	$f_\mathrm{u}\Delta t$	N	S	R	$\max_r \lvert\hat{f}_r^{\mathrm{FD}} - f_r^{\mathrm{EP}}\rvert/\lvert f_r^{\mathrm{EP}}\rvert$
A	–	0.0720	3072	70	17	5.5×10^{-8}
B	0.0720	0.0935	3072	74	18	1.5×10^{-9}
C	0.0935	0.1085	5120	94	23	1.3×10^{-9}
D	0.1085	0.1280	7168	194	48	2.1×10^{-9}
E	0.1280	0.1460	12288	246	61	2.3×10^{-8}

The frequency domain subspace algorithm uses the parameters f_l, f_u, N, S and R to give estimates $\hat{f}_r^{\mathrm{FD}}$ which are compared to f_r^{EP} computed from the corresponding eigenvalue problem formulated in the frequency domain.

reduces the overall computation time with at least a factor 94 as compared to a standard DFT, possibly, in combination with a Padé approximation. In terms of accuracy for such a situation, the frequency domain subspace algorithm clearly outperforms the DFT/Padé-technique [11,12], which typically gives a relative error of a couple per mille.

4.3. Test 3 – Cavity with aperture in free space

The third and last test case is a free-space computation for a PEC cavity with an aperture. Specifically, we use the brick shaped cavity described in Section 4.1 (with $\sigma = 0$) and create an aperture in the wall at $y = l_y$ by removing the square defined by $l_x - d < x < l_x$ and $l_z - d < z < l_z$, where $d = 4$ mm. We exploit the FDTD scheme to compute the electromagnetic fields, which are excited by the current loop shown in Fig. 4. The fields are sampled at a number of randomly selected points inside the cavity and we use the frequency domain subspace algorithm to estimate the resonant frequencies and the Q-factors of the cavity with the aperture. The opened cavity is put at the center of a simulation box with metal walls and the outward propagating wave is effectively absorbed by a sponge layer [29] which covers the truncating walls of the simulation box. The free-space region in-between the cavity and the sponge layer measures 8 mm along the Cartesian axis and the sponge layer is 8 mm thick.

We discretize the computational domain with the cell size $h = 1/4$ mm and select the time step $\Delta t = h/\sqrt{3}c_0$. The spectrum of the excitation is chosen such that it would energize only the 25 lowest

Table 4
Estimated damping rates, resonant frequencies and quality factors of the 25 lowest resonances of a brick shaped cavity with an aperture

Cavity with aperture			Closed cavity
$\hat{\gamma}_r$ (GHz)	$\hat{f}_r$ (GHz)	$\hat{Q}_r$ (–)	f_r (GHz)
5.0060×10^{-3}	14.498	9.0986×10^{3}	14.515
1.5920×10^{-2}	16.203	3.1975×10^{3}	16.230
1.9234×10^{-2}	17.817	2.9102×10^{3}	17.849
8.6146×10^{-2}	19.820	7.2280×10^{2}	19.909
2.1109×10^{-2}	19.883	2.9590×10^{3}	19.909
4.4507×10^{-2}	21.023	1.4840×10^{3}	21.067
9.4405×10^{-2}	22.234	7.3989×10^{2}	22.284
1.7637×10^{-1}	24.613	4.3841×10^{2}	24.682
3.0030×10^{-1}	24.963	2.6115×10^{2}	25.092
6.0868×10^{-2}	25.058	1.2933×10^{3}	25.092
3.2613×10^{-1}	26.660	2.5682×10^{2}	26.780
6.4300×10^{-1}	27.992	1.3677×10^{2}	28.196
3.4987×10^{-1}	28.105	2.5237×10^{2}	28.196
9.5757×10^{-2}	28.613	9.3873×10^{2}	28.631
4.4163×10^{-1}	28.743	2.0447×10^{2}	28.845
1.1421×10^{-1}	28.926	7.9568×10^{2}	29.025
2.0803×10^{-1}	29.525	4.4587×10^{2}	29.581
1.5056×10^{-1}	29.720	6.2013×10^{2}	29.746
6.3299×10^{-1}	30.740	1.5257×10^{2}	30.868
4.4013×10^{-2}	30.863	2.2030×10^{3}	30.868
1.6539	31.647	6.0118×10^{1}	31.905
1.8535×10^{-1}	31.897	5.4064×10^{2}	31.905
3.2302×10^{-1}	31.966	3.1089×10^{2}	32.068
5.2019×10^{-2}	31.976	1.9312×10^{3}	32.068
1.9906×10^{-1}	32.429	5.1180×10^{2}	32.452

The resonant frequencies for the corresponding closed cavity are included for comparison.

eigenmodes of the corresponding closed cavity, i.e., the time-dependence is based on a lowpass filter with $f_p\Delta t = 0.0156$ and $f_s\Delta t = 0.0164$. We exploit the frequency domain subspace algorithm to estimate the resonances in the interval $0 \leqslant f\Delta t < 0.0185$. We set the auxiliary model order $S = 204$ and use 8192 samples in time from six different points inside the cavity for the estimation. We find that $R/2 = 25$, which is clearly shown by the distribution of the singular values computed from Eq. (18). The estimated damping rates, resonant frequencies and Q-factors are listed in Table 4, which also includes the eigenfrequencies computed from Eq. (24) for the corresponding closed cavity in the same setting.

For all estimated quantities in Table 4, we tentatively estimate that the relative error due to the frequency domain subspace algorithm is less than 10^{-4}. This error can be reduced significantly by increasing N and/or S as previously demonstrated. Additional FDTD computations with $h = 1$, 1/2 and 1/3 mm indicated that the discretization errors introduced by the FDTD scheme when $h = 1/4$ mm is less than 5×10^{-4} for the complex frequencies $\hat{\beta}_r = -\hat{\gamma}_r + \mathrm{i}2\pi\hat{f}_r$. However, the relative error for the damping rates $\hat{\gamma}_r$ and the quality factors $\hat{Q}_r$ are roughly estimated to be in the range from 3% to 12%. Again, the error introduced by the frequency domain subspace algorithm can be made negligible as compared to the discretization errors of a numerical scheme based on linear elements.

The signal model (2) allows for extrapolation of the sampled signal with respect to time. Consequently, the complete response of a system can be determined inexpensively from a relatively short computation by joining the non-autonomous part of the response with the autonomous part computed from the signal model (2). To demonstrate this technique, we estimate the amplitudes $\hat{\mathbf{a}}_r$ in the signal model by linear regression. The signal model is then evaluated for 150,000 time steps, which also includes the portion that was used for the estimation. We compare this result with the output from the standard FDTD computation for the same time interval. The comparison is performed in terms of a moving root-mean-square (RMS) measure $m(n; y, \delta_m) = [(2\delta_m + 1)^{-1} \sum_{v=n-\delta_m}^{n+\delta_m} (y(v))^2]^{1/2}$, where δ_m defines the length of the moving interval used for the RMS value. In Fig. 9, the curve labeled A shows the moving RMS measure $m(n; y_1, 100)$, where y_1 is the first component of $\mathbf{y}$ as computed by the FDTD scheme. The RMS measure of the error for the

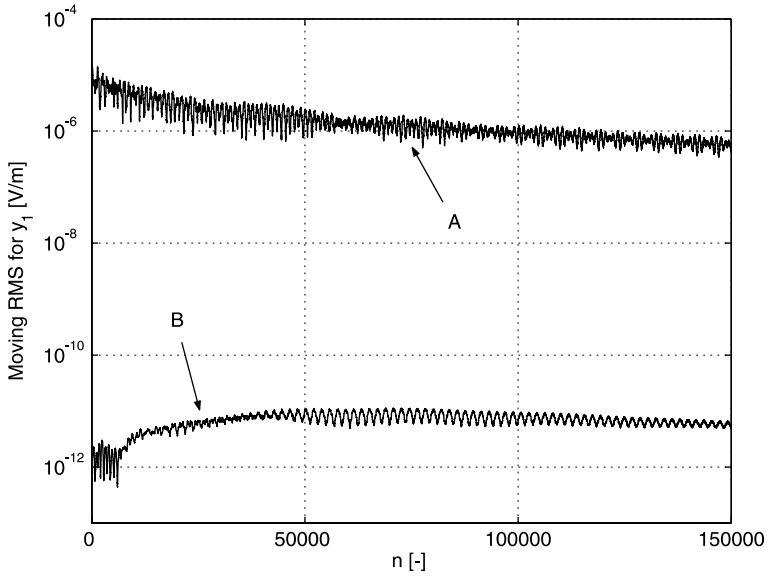

Fig. 9. The curve labeled A shows the moving RMS measure $m(n; y_1, 100)$ and B shows $m(n; \hat{y}_1 - y_1, 100)$, where y_1 is the first component in the sampled data $\mathbf{y}$ as computed by the FDTD scheme. The moving RMS is defined as $m(n; y, \delta_m) = [(2\delta_m + 1)^{-1} \sum_{v=n-\delta_m}^{n+\delta_m} (y(v))^2]^{1/2}$.

corresponding estimated time signal $\hat{y}_1$ is given from $m(n; \hat{y}_1 - y_1, 100)$ and it is shown by the curve labeled B in Fig. 9. By virtue of the frequency domain subspace algorithm combined with the frequency selective excitation, we achieve a relative error (measured in terms of the moving RMS) in the estimated time domain signal which is roughly of the order 10^{-5} for the first 150,000 time steps.

The brute force FDTD computation needed 100 h to complete, which includes 10,590 time steps for the excitation and the additional 150,000 time steps for the autonomous system. It takes 1.4×10^6 time steps for the signal y_1 to decay to 10^{-5} of its maximum amplitude and a straight forward FDTD computation would require roughly 36 days to complete. The frequency domain subspace algorithm needs only 8192 time steps to estimate the frequencies and amplitudes of the signal model and together with the time steps used for the excitation the total computation time is less than 12 h. The frequencies and amplitudes are estimated by the frequency domain subspace algorithm in 6 s. All computations were performed on an ordinary desktop PC.

5. Conclusion

We have presented and tested a new frequency domain subspace algorithm for the estimation of resonant frequencies and quality factors from the output produced by time domain computations. The method can be interpreted as a frequency domain version of the well known ESPRIT algorithm. It uses a subset of the DFT computed from the time domain data, where the selected DFT frequencies reside in the frequency band of interest. This gives two advantages: (a) working on a subset of data lowers both the computation time and the memory requirements, and (b) the selection of DFT points from a sub-band corresponds to a band-pass filtering operation which suppresses out-of-band signals. The algorithm gives no transient effects, which are inevitable using standard time domain filtering techniques. Thus, it is completely insensitive to the normally troublesome spectral leakage phenomenon.

It was demonstrated by numerical tests, given a lossless and brick shaped cavity, that the frequency domain subspace algorithm can simultaneously estimate the lowest 80 eigenfrequencies (excluding degeneracy) with a relative error well below 10^{-12}. These results were reproduced for the same cavity filled with a material characterized by a homogeneous conductivity, which translates into Q-factors in the range from 80 to 300. For lower Q-factors, the simultaneous estimation of 80 eigenfrequencies gives reduced accuracy. However, it is possible to concurrently compute accurate estimates for ten resonances with Q-factors as low as unity.

We also suggested an efficient procedure to generate the temporal dependence for relatively short excitations with an a priori selected frequency spectrum. This technique provides us with a very effective alternative to suppress unwanted resonances, which is useful for time domain computations in general. The procedure exploits the well established digital filter design techniques first developed for signal processing problems. Specifically, the discrete time dependence of the excitation is set to the impulse response of an appropriate digital filter. The roll off and stop-band ripple of a low order filter can, with a low computational cost, be improved significantly by using the impulse response of the filter as the input to the filter itself. Such an excitation has a dynamic range which makes the stop-band magnitude essentially zero, as compared to the pass-band, for computations with 16 digits of precision.

The frequency domain subspace algorithm was exploited to estimate the resonant frequencies for a lossless three-dimensional bow-tie microwave resonator. We extracted the 167 lowest resonant frequencies from only two FEM computations with, in total, less than 23,000 time steps. The relative deviation in the estimated frequencies is less than 10^{-7} as compared to the equivalent eigenfrequencies computed from the standard eigenvalue problem formulated in the frequency domain. Here, a straightforward DFT requires at least two orders of magnitude more time steps to resolve the interval in-between the two closest spaced resonances with three DFT points. The DFT combined with a Padé approximation typically achieves a relative error on the order of one per mille.

Given accurate estimates of the excited frequencies and dampings, it is a straightforward linear regression problem to determine the corresponding amplitudes, although these are generally less accurately estimated than the frequencies. Having all signal parameters available makes it possible to cheaply compute the continuation of the time domain signal for an arbitrary number of subsequent time steps. One important application is, e.g., the computation of scattering parameters of systems with weakly damped modes. To test this, we performed a free-space computation for a cavity with an aperture. The estimated frequencies, dampings and amplitudes were used to evaluate the time domain signal beyond the initial 8192 time steps used for the estimation itself. The relative error (measured as a moving RMS) in the extrapolated time domain signal was found to be roughly 10^{-5} for the first 150,000 time steps. The extrapolation of the time domain signal reduces the overall computer time with almost two orders of magnitude as compared to a standard DFT where it is assumed that the final amplitude of the extrapolated response is required to be reduced to a factor 10^{-5} of its maximum (in the moving RMS sense).

The frequency domain subspace algorithm decouples the estimation of frequencies and amplitudes from the time domain differential equation solver. Thus, it is feasible to use a wide range of advanced and highly efficient time domain solvers, including hybrid schemes, without the need of reverting to a corresponding frequency domain formulation. By virtue of the high accuracy in the frequency estimates, the proposed algorithm can be used in conjunction with higher order schemes and/or for extrapolation to zero cell size. The frequency domain subspace algorithm is general in nature and, therefore, applicable to estimation problems found in any applications involving harmonics, e.g., electrical circuit-theory, telecommunications, acoustics, solid mechanics and quantum mechanics.

Acknowledgements

Thomas Rylander was supported in part by the Air Force Office of Scientific Research under a Grant F49620-01-1-0228 and in part by grants from the National Graduate School in Scientific Computing (NGSSC) and the Swedish Research Council on Engineering Science (TFR). Tomas McKelvey and Mats Viberg were in part supported by the Swedish Research Council (VR).

References

[1] K.S. Yee, Numerical solution of initial boundary value problems involving Maxwell's equations in isotropic media, IEEE Trans. Antennas Propagat. 14 (1966) 302–307.
[2] A. Taflove, Computational Electrodynamics: The Finite-Difference Time-Domain Method, Artech House, Norwood, MA, 1995.
[3] J.M. Jin, The Finite Element Method in Electromagnetics, second ed., Wiley, New York, NY, 2002.
[4] W.C. Chew, J.M. Jin, E. Michielssen, J. Song, Fast and Efficient Algorithms in Computational Electromagnetics, Artech House, Norwood, MA, 2001.
[5] S.M. Kay, Modern Spectral Estimation: Theory and Application, Prentice-Hall, Englewood Cliffs, NJ, 1988.
[6] P. Stoica, R.L. Moses, Introduction to Spectral Analysis, Prentice-Hall, Englewood Cliffs, NJ, 1997.
[7] W.L. Ko, R. Mittra, A combination of FD-TD and Prony's methods for analyzing microwave integrated circuits, IEEE Trans. Microwave Theory Tech. 39 (1991) 2176–2181.
[8] J.A. Pereda, L.A. Vielva, A. Vegas, A. Prieto, Computation of resonant frequencies and quality factors of open dielectric resonators by a combination of the finite-difference time-domain (FDTD) and Prony's methods, IEEE Microwave Guided Wave Lett. 2 (1992) 431–433.
[9] A.K. Shaw, K. Naishadham, ARMA-based time-signature estimator for analyzing resonant structures by the FDTD method, IEEE Trans. Antennas Propagat. 49 (2001) 327–339.
[10] W.H. Press, S.A. Teukolsky, W.T. Vetterling, B.P. Flannery, Numerical Recipes in C: The Art of Scientific Computing, Second ed., Cambridge University Press, New York, NY, 1992.
[11] S. Dey, R. Mittra, Efficient computation of resonant frequencies and quality factors of cavities via a combination of the finite-difference time-domain technique and the Padé approximation, IEEE Microwave Guided Wave Lett. 8 (1998) 415–417.

[12] T. Rylander, A. Bondeson, Stable FEM-FDTD hybrid method for Maxwell's equations, Comput. Phys. Commun. 125 (2000) 75–82, doi:10.1016/S0010-4655(99)00463-4.
[13] S.Y. Kung, A new identification and model reduction algorithm via singular value decompositions, in: Proceedings of the 12th Asilomar Conference on Circuits, Systems and Computers, Pacific Grove, CA, 1978, pp. 705–714.
[14] R. Roy, T. Kailath, ESPRIT – estimation of signal parameters via rotational invariance techniques, IEEE Trans. Acoust., Speech Signal Process. 37 (1989) 984–995.
[15] R.O. Schmidt, Multiple emitter location and signal parameter estimation, IEEE Trans. Antennas Propagat. 34 (1986) 276–280.
[16] Z. Bi, Y. Shen, K. Wu, J. Litva, Fast finite-difference time-domain analysis of resonators using digital filtering and spectrum estimation techniques, IEEE Trans. Microwave Theory Tech. 40 (1992) 1611–1619.
[17] F. Liu, J.E. Schutt-Ainé, J. Chen, Full-wave analysis and modeling of multiconductor transmission lines via 2-D-FDTD and signal-processing techniques, IEEE Trans. Microwave Theory Tech. 50 (2002) 570–577.
[18] T. McKelvey and M. Viberg, A robust frequency domain subspace algorithm for multi-component harmonic retrieval, in: Proceeedings of the 35th Asilomar Conf. Sig. Sys. Comput., Pacific Grove, CA, 2001, pp. 1288–1292.
[19] M. Verhaegen, P. Dewilde, Subspace model identification. Part I: the output-error state-space model identification class of algorithms, Int. J. Control 56 (1992) 1187–1210.
[20] M. Viberg, Subspace-based methods for the identification of linear time-invariant systems, Automatica 31 (1995) 1835–1851.
[21] T. McKelvey, H. Akçay, L. Ljung, Subspace-based multivariable system identification from frequency response data, IEEE Trans. Automat. Control 41 (1996) 960–979.
[22] G.H. Golub, C.F. van Loan, Matrix Computations, second ed., The Johns Hopkins University Press, Baltimore, MD, 1989.
[23] M. Haardt, J. Nossek, Unitary ESPRIT: how to obtain increased estimation accuracy with a reduced computational burden, IEEE Trans. Signal Process. 43 (1995) 1232–1242.
[24] B. Boashash, Estimating and interpreting the instantaneous frequency of a signal. Part I: Fundamentals, Proc. IEEE 80 (1992) 520–538.
[25] J.C. Nédélec, Mixed finite elements in R^3, Numer. Math. 35 (1980) 315–341.
[26] J.F. Lee, R. Lee, A. Cangellaris, Time-domain finite-element methods, IEEE Trans. Antennas Propagat. 45 (1997) 430–442.
[27] S. Balay, K. Buschelman, W.D. Gropp, D. Kaushik, M. Knepley, L. Curfman McInnes, B.F. Smith, H. Zhang, PETSc home page. Available from: <http://www.mcs.anl.gov/petsc>.
[28] R.B. Lehoucq, D.C. Sorensen, C. Yang, ARPACK Users' Guide: Solution of Large-Scale Eigenvalue Problems with Implicitly Restarted Arnoldi methods, SIAM, Philadelphia, PA, 1998.
[29] P.G. Petropoulos, L. Zhao, A.C. Cangellaris, A reflectionless sponge layer absorbing boundary condition for the solution of Maxwell's equations with high-order staggered finite difference schemes, J. Comput. Phys. 139 (1998) 184–208, doi:10.1006/jcph.1997.5855.